

Mechanisms for Long-Lived, Photo-Induced Superconductivity

Sambuddha Chattopadhyay,¹ Christian J. Eckhardt,^{2,3} Dante M. Kennes,^{2,3} Michael A. Sentef,^{4,3} Dongbin Shin,^{3,5} Angel Rubio,³ Andrea Cavalleri,^{3,6} Eugene A. Demler,⁷ and Marios H. Michael³

¹*Lyman Laboratory, Department of Physics, Harvard University, Cambridge, MA 02138, USA*

²*Institut für Theorie der Statistischen Physik, RWTH Aachen University and JARA-Fundamentals of Future Information Technology, 52056 Aachen, Germany*

³*Max Planck Institute for the Structure and Dynamics of Matter, Center for Free-Electron Laser Science (CFEL), Luruper Chaussee 149, 22761 Hamburg, Germany*

⁴*H H Wills Physics Laboratory, University of Bristol, Bristol BS8 1TL, United Kingdom*

⁵*Gwangju Institute of Science and Technology, 123 Cheomdangwagi-ro, Buk-gu, Kwangju, South Korea*

⁶*Department of Physics, Clarendon Laboratory, University of Oxford, United Kingdom*

⁷*Institute for Theoretical Physics, ETH Zürich, 8093 Zürich, Switzerland*

(Dated: March 28, 2023)

Advances in the control of intense infrared light have led to the striking discovery of metastable superconductivity in K_3C_{60} at 100K, lasting more than 10 nanoseconds. Inspired by these experiments, we discuss possible mechanisms for long-lived, photo-induced superconductivity above T_c . We analyze a minimal model of optically-driven Raman phonons coupled to inter-band electronic transitions. Using this model, we develop a possible microscopic mechanism for photo-controlling the pairing interaction by displacively shifting the Raman mode. Leveraging this mechanism, we explore two pictures of long-lived, light-induced superconductivity far above T_c . We first investigate long-lived, photo-induced superconductivity arising from the metastable trapping of a displaced phonon coordinate. We then propose an alternate route to long-lived superconductivity. Within this paradigm, the slow equilibration of quasi-particles enables a long-lived, non-thermal superconducting gap. We conclude by discussing implications of both scenarios to experiments that can be used to discriminate between them. Our work provides falsifiable, mechanistic explanations for the nanosecond scale photo-induced superconductivity found in K_3C_{60} , while also offering a theoretical basis for exploring long-lived, non-equilibrium superconductivity in other quantum materials.

INTRODUCTION

Breakthroughs in the structural control of matter using intense, infrared (IR) light have enabled the exploration of quantum order outside of the confines of thermal equilibrium^{1,2}. From photo-induced ferroelectricity in $SrTiO_3$ ^{3,4} to driven charge density wave ordering in $LaTe_3$ ^{5,6} to optically-stabilized ferromagnetism in $YTiO_3$ ⁷ to transient, light-induced superconductivity in layered cuprates^{8,9}, a striking array of experiments have traced a path towards the photo-control of complex, quantum materials, a focal project for modern condensed matter.

Arguably the most captivating experiment in this field is the metastable superconductivity uncovered in K_3C_{60} , far above T_c ^{10–12}. In the K_3C_{60} experiments, intense pulses of mid-IR light induced optical signatures of superconductivity at $T = 100K$ ($T_c = 20K$) which lasted over 10 nanoseconds, 1,000 times longer than any microscopic time-scale in the experiment. The longevity of this response after driving should be contrasted with the transient superconductivity observed in, e.g., driven cuprates⁸, where superconducting signatures in the optical conductivity dissipate within the picosecond scale ring-down time of the resonantly driven apical oxygen modes (for theoretical investigations motivated by these experiments, see Refs.^{13–29}). The K_3C_{60} experiments thus open up the tantalizing possibility of *long-lived*,

photo-induced superconductivity at high temperatures.

Galvanized by the experiments performed in K_3C_{60} , we explore possible mechanisms for light-induced, long-lived superconductivity. Within a generic, experimentally relevant minimal model, we develop a microscopic mechanism for photo-induced superconductivity. We consider photo-distorting a local Raman phonon coupled to the inter-band transition between two narrow electronic bands, shown schematically in Fig. 1. We show that photo-inducing structural modifications by displacively shifting a local Raman phonon leads to an enhancement of the attractive interaction, providing a knob for photo-controlling superconductivity.

We subsequently lay out two distinct explanations for non-equilibrium superconductivity that persists long after driving, presenting distinct emergent life-times for non-equilibrium superconductivity. We first compute the adiabatic free energy landscape of our model as a function of the induced structural distortion and find that in physically plausible parameter regimes metastable superconductivity at finite phonon distortion exists far above T_c and can be accessed through laser driving (see Figure 2). We next advance an alternate route to long-lived, light-induced superconductivity that does not rely on metastable trapping. We argue that photo-inducing a large superconducting gap during driving can lead to bottlenecks in the equilibration of quasi-particles; the slow equilibration of quasi-particles then yields a long-lived,

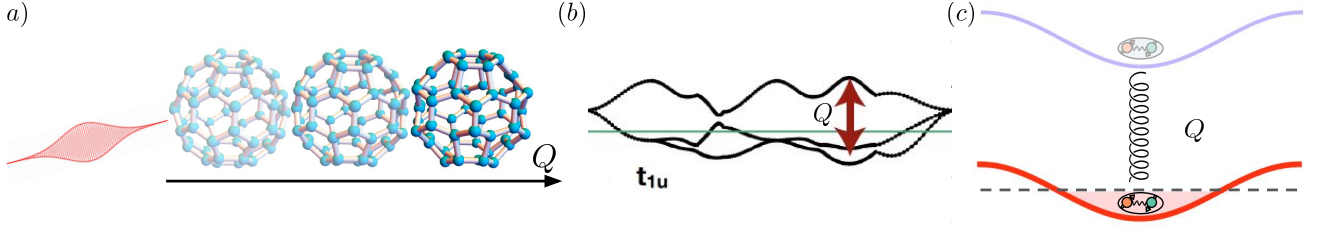


FIG. 1. **Mechanism for Photo-Induced Superconductivity** Sketch of the inter-band phonon coupling mechanism that can give rise to light-induced, long-lived superconductivity using K_3C_{60} as an example. (a) Schematic of the pumping mechanism, where a laser pulse induces a displacive shift of the Raman coordinate Q during the pulse duration. For illustration we use the Jahn-Teller Hg(3) mode of K_3C_{60} . (b) In K_3C_{60} , particular Jahn-Teller Hg mode polarizations couple the occupied and unoccupied t_{1u} bands near the Fermi energy. (c) To capture the essential physics of this mechanism, we study a two band model with a phonon coupled to the interband transition. We find that a photo-induced static shift of a Raman mode hybridizes the upper and lower bands, thereby photo-enhancing superconductivity.

non-thermal superconducting gap above T_c . Crucially, we find that both pictures are plausible for experiments in alkali-doped fullerenes—we conclude by exploring the implications of each to the experiments.

MODEL

Inspired by aspects relevant to superconductivity in alkali-doped fullerenes—strong, local electron-phonon coupling and narrow bands—we begin with a generic minimal model that couples dispersionless optical Raman phonons to the local inter-orbital transition between two electronic states. The electrons are allowed to weakly hop across sites on a three-dimensional lattice. We examine the Hamiltonian H , given by

$$H = H_0 + H_{int} + H_K, \quad (1)$$

where the free part of the Hamiltonian, H_0 is given by

$$H_0 = -\frac{\Delta E}{2} \sum_{i,\sigma} (c_{i,\sigma}^\dagger c_{i,\sigma} - d_{i,\sigma}^\dagger d_{i,\sigma}) + \sum_i \frac{P_i^2}{2M} + \frac{M\omega^2}{2} Q_i^2 \quad (2)$$

while the electron-phonon coupling is given by the interaction:

$$H_{int} = g \sum_{i,\sigma} Q_i (c_{i,\sigma}^\dagger d_{i,\sigma} + d_{i,\sigma}^\dagger c_{i,\sigma}), \quad (3)$$

and where the (weak) nearest neighbor hopping Hamiltonian is $H_K = -t \sum_{\langle i,j \rangle, \sigma} (c_{i,\sigma}^\dagger c_{j,\sigma} + d_{i,\sigma}^\dagger d_{j,\sigma} + h.c.)$. Here $c_{i,\sigma}^\dagger (c_{i,\sigma})$ creates (annihilates) a c -electron with spin $\sigma \in \{\uparrow, \downarrow\}$ at site i ; $d_{i,\sigma}^\dagger (d_{i,\sigma})$ creates (annihilates) a d -electron with spin σ at site i ; P_i and Q_i are the momentum and position coordinates for a phonon of frequency ω and mass M at site i ; ΔE is the splitting between levels c and d ; and g is the electron-phonon coupling. We con-

sider a system in which the c -electrons are partially filled at equilibrium. While this Hamiltonian has been considered in the context of superconductivity in $SrTiO_3$ ³⁰, its implications on photo-induced superconductivity have not been explored.

We consider what happens when the mean local Raman coordinate $\langle Q \rangle$, is homogeneously displaced by intense mid-IR laser light. As they are inversion symmetric, Raman modes are driven by the laser non-linearly through the Hamiltonian, $H_R \propto E^2(t)Q$ where $E(t)$ is the electric field of the laser light (e.g. via their Raman activity³¹ or anharmonic coupling with linearly driven IR-active modes³²). Non-linear driving induces a shift in the average position of the Raman modes during the pump pulse, a phononic equivalent of optical rectification.

Displacing $\langle Q \rangle$ hybridizes the upper and lower bands. In the limit of $g \langle Q \rangle \ll \Delta E$, shifting $\langle Q \rangle$ facilitates virtual, inter-orbital transitions between occupied c and unoccupied d levels. A pair of c electrons at the same site can then take advantage of energetic benefit of this facilitated virtual tunneling and form a local, singlet pair. As this tunneling depends explicitly on $\langle Q \rangle$, so too will the pairing interaction—a photo-tunable virtual Suhl-Kondo effect^{33,34}. We rigorize the intuition presented by deriving, for instantaneous values of $\langle Q \rangle$, an attractive Hubbard Hamiltonian for effective lower-band f electrons, of the form:

$$H_{eff} = \sum_{k,\sigma} \xi_k f_{k,\sigma}^\dagger f_{k,\sigma} - \frac{U}{N} \sum_{\substack{k,k' \\ |\xi_k|, |\xi_{k'}| < \omega}} f_{k,\uparrow}^\dagger f_{-k,\downarrow}^\dagger f_{k',\uparrow} f_{-k',\downarrow}, \quad (4)$$

where $\xi_k = \epsilon_k - \mu$, where ϵ_k is the free electron energy dispersion. For a fixed value of $\langle Q \rangle$, we find that the induced attraction is given by:

$$U = U_0 + \frac{g^2}{M\omega^2} \frac{4g^2 \langle Q \rangle^2}{\Delta_{eff}^2}, \quad (5)$$

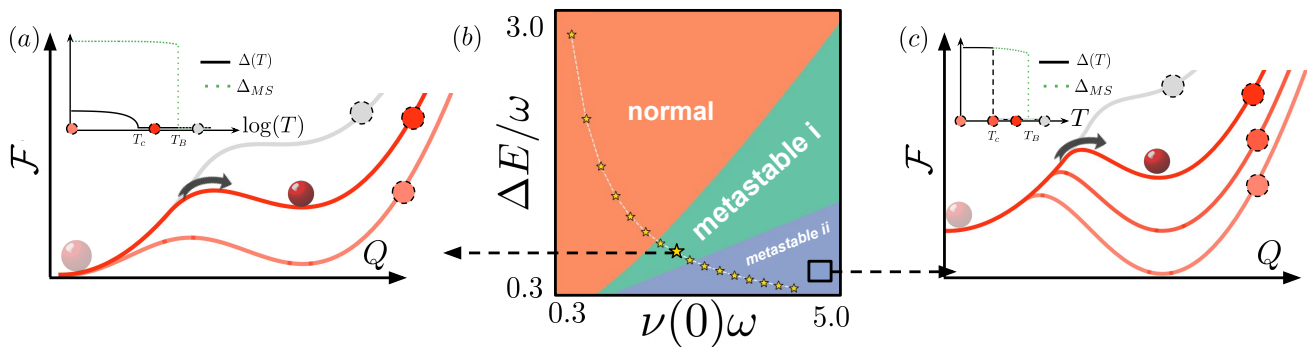


FIG. 2. **Metastable Superconductivity** Phase diagram (b) for metastable superconductivity at fixed electron-phonon coupling $\frac{g\ell_0}{\omega} = 0.6$ and (second order) $T_c = 20K$ as a function of the level splitting ΔE and density of states at the Fermi level $\nu(0)$, showcasing distinct regimes of metastability—metastable I (green) and metastable II (blue). T_c is fixed by choosing U_0 such that $\lambda_{eff}(Q=0) = U_0\nu(0) = 0.3$. The white curve, with stars, traces the parameter range relevant to K_3C_{60} . Variance in ΔE and $\nu(0)$ arises due to uncertainty in the degree to which Brinkmann-Rice effects renormalize the bandwidth (see “Photo-Induced Metastability” in the Discussion). Schematic free energy landscape for metastable I (a), depicted across three temperatures— $T=0$ (light red), $T > T_c$ (dark red), $T > T_B$ (grey). By driving Q over the free energy barrier, one can access a metastable superconducting state starting from $T=0$, continuing through the equilibrium T_c , until $T=T_B$ where it becomes untrapped. The hidden state has a larger metastable superconducting gap Δ_{MS} : see the inset for a comparison with the gap in thermal equilibrium as a function of temperature. Schematic free energy landscape for metastability II (c), caricatured across four temperatures: $T=0$ (lightest red), $T=T_c$ (light red), $T > T_c$ (dark red), and $T > T_B$. Here, the distorted state with larger gap is the ground state: metastability II implies a first order phase transition at $T=T_c$. Above T_c , metastable superconductivity is accessible until T_B (inset).

where $\Delta_{eff} = \sqrt{\Delta E^2 + 4g^2 \langle Q \rangle^2}$ and U_0 is attractive interaction arising from extrinsic pairing mechanisms that yield superconductivity for the undistorted material. We derive the $\langle Q \rangle$ -dependent enhancement of U in the Supplemental Material³⁵, through a diagonalizing rotation, followed by a Schrieffer-Wolff transformation performed on H_{int} to fully remove the lowest order terms in the electron-phonon coupling. Shifting the mean local phonon coordinate by laser driving thus provides a dynamical handle for photo-enhancing superconductivity.

PHOTO-INDUCED METASTABILITY

We now explore the simplest quasi-equilibrium picture for long-lived, light-induced superconductivity: optically driving the material into a hidden, thermodynamically metastable phase². We study the driven, dissipative dynamics of the mean phonon coordinate $\langle Q \rangle$ —hereafter in this section Q —in an adiabatic free energy landscape that captures the trade-off between the free-energy benefit of inducing a displacive shift Q —leading to enhanced U and a stronger superconductor—and the elastic cost of such a distortion. Using a finite-temperature BCS ansatz for the electrons, we model the evolution of Q as:

$$\left(\partial_t^2 + \gamma \partial_t + \frac{1}{M} \frac{\partial \mathcal{F}_{SC}}{\partial Q} + \omega^2 \right) Q = zE^2(t) + \eta(t), \quad (6)$$

where $zE^2(t)$ is the effective displacive acceleration arising from laser driving; where $\eta(t)$ is fluctuation-

dissipation obeying white noise with $\langle \eta(t)\eta(t') \rangle = 2\frac{\gamma}{M}T\delta(t-t')$; and where the BCS superconducting free-energy density \mathcal{F}_{SC} is given by:

$$\mathcal{F}_{SC} = \frac{\Delta^2}{U} - 2\nu(0) \int_0^\omega d\xi \left(\sqrt{\xi^2 + \Delta^2} - \xi \right) - 4\nu(0)T \int_0^\omega d\xi \ln \left(1 + e^{-\beta\sqrt{\xi^2 + \Delta^2}} \right). \quad (7)$$

Here $\nu(0)$ is the density of states per spin per site at the Fermi-level and $\Delta(Q)$ is obtained by solving the BCS self-consistency equation for $U(Q)$.

We start with a system without a shift ($Q=0$), in the normal state, at finite temperature $T > T_c$. We assume that the drive is sufficiently strong to traverse any free-energy barrier between the global free-energy minimum at $Q=0$ and the putative, superconducting metastable state at $Q_{MS} \neq 0$. After driving the phonon coordinate into such a metastable trap, a return to equilibrium through macroscopic nucleation due to thermal fluctuations is, canonically, slow. Our goal is thus to ascertain when the free energy landscape has a non-trivial local minimum. A sufficient condition for the free energy landscape to host a metastable state is that $T=0$ energy landscape should have a non-trivial local minimum. For $U_0=0$, a metastable state exists if:

$$Q_c^2 = \frac{\Delta E}{\sqrt{2}g^2} \omega \Delta(Q_c), \quad (8)$$

has two positive solutions Q_B and Q_{MS} , corresponding to a local maximum and minimum in the energy landscape,

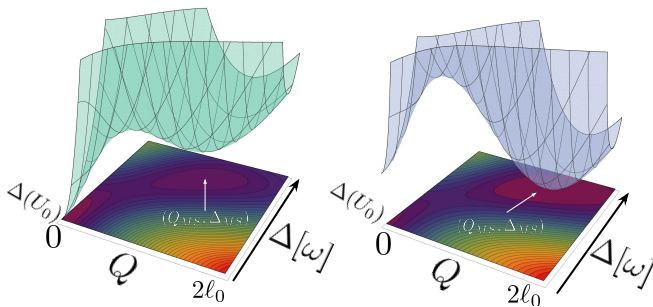


FIG. 3. **Comparing Metastabilities** Free energy (eq. 7) landscape as a function of Δ and Q , in units of ω and $\ell_0 = \frac{1}{\sqrt{m\omega}}$, at $T \ll T_c$. In both cases there are two local free energy minima: the undistorted state $(Q, \Delta) = (0, \Delta(U_0))$ and the (meta)-stable distortion (Q_{MS}, Δ_{MS}) . In each case, $\Delta_{MS} > \Delta(U_0)$. (Left) Metastable I: The undistorted state is the global free energy minimum. (Right) Metastable II: The distorted state, with a larger gap, is the equilibrium state at low temperatures.

respectively. Metastability persists until T_B where the free energy landscape no longer has non-trivial critical points and the metastable state becomes untrapped, as shown by the grey landscapes in Fig. 2(a) & (c).

We now distinguish between two types of metastability with a phase diagram delimiting their boundaries provided in Fig. 2(b). The first type, metastability I, corresponds to the scenario in which $E(Q_{MS}) > E(0)$, where $E(Q) = \frac{1}{2}M\omega^2Q^2 - \omega^2\nu(0)\coth\left(\frac{1}{\nu(0)U(Q)}\right)$ (see Fig. 2(a)). In this scenario, the distortionless, normal state is always the equilibrium state and metastability occurs between $0 < T < T_B$. The alternate scenario, metastability II, occurs when at $T = 0$ a distorted ground state is energetically favorable (see Fig. 2(c)). Equilibrium superconductivity exists until a critical temperature T_c where a first order phase transition occurs and the superconductivity-inducing distortion is no longer free energetically favorable. In metastability II, optically switched superconductivity is possible for $T_c < T < T_B$. A prominent experimental signature accompanying metastability II is the presence of a distortion-driven, first-order superconducting phase-transition. In passing, we note that while our approach near the local maximum is within BCS, the precise position of the local minima, thereby the quantitative boundary between metastability I & II, may require a treatment beyond BCS to capture the effects of strong fluctuations.

QUASI-PARTICLE TRAPPING

While long-lived superconductivity arising from the metastable trapping of a displaced phonon coordinate is a natural mechanism to explore, it is not the only route to long-lived, light-induced superconductivity. In what follows, we consider the equilibrating dynamics of quasi-

particles through a slow displacement of the phonon in a free energy landscape without a metastable trap.

We begin by considering an undistorted superconductor in its metallic phase at $T > T_c$. We then imagine displacing Q to a large Q^* , inducing an attraction U^* , where—for simplicity—it is held long enough to thermalize to a finite-temperature superconductor with a gap $\Delta(Q^*, T)$ and quasi-particle density number n^* . After the drive shuts off, given the lack of a metastable trap, the phonon coordinate relaxes to $Q = 0$. This relaxation—while fast compared to the life-time of the superconductivity—occurs over the $10ps$ scale ring-down time of the Raman mode. For sufficiently large superconducting gaps $\Delta(Q^*, T)$, non-adiabatic heating of quasi-particles as the interaction $U(Q)$ changes is negligible—this is the case for experiments in K_3C_{60} , where we expect at least terahertz-scale superconducting gaps¹¹. As U is lowered back to its equilibrium value, in order for the electrons to relax back to equilibrium, quasi-particles need to be generated out of the condensate. We argue that this process is slow.

The relaxation of quasi-particles is predominantly due to scattering between quasi-particles and thermally populated, low energy phonons. Crucially, a (large) superconducting gap can make scattering processes that conserve quasi-particle number dramatically faster than those which alter the quasi-particle number. In particular, while number-conserving quasi-particle scattering can involve phonons at arbitrarily low energies, the generation of quasi-particles out of the condensate requires the absorption of phonons above 2Δ . Such a “phonon bottleneck” can emphatically slow down the generation of quasi-particles. Thus, if as the phonon relaxes, the gap remains large, we can approximate this evolution for the electrons as one in which the quasi-particle density remains frozen at n^* : if a large $\Delta(Q^*)$ was opened up during driving, n^* could be vanishingly small. Therefore, even though pairing strength is lowered to a level that is insufficient to generate a finite gap in thermal equilibrium, phonon bottlenecks in the equilibration of the quasi-particle density generate a non-thermal distribution of quasi-particles, which in turn enables superconductivity over the long time-scale that it takes for quasi-particles to be generated out of the condensate. We thus present *quasi-particle trapping*: a paradigm for long-lived, non-equilibrium superconductivity without thermodynamic metastability.

We now formalize the conceptual picture above. We consider displacing Q from 0 to Q^* , holding it there, and creating a superconductor with gap $\Delta(Q^*, T)$ and density n^* of Bogolyubov quasi-particles. After the phonon coordinate relaxes to $Q = 0$, we are left with the undriven pairing strength U_0 , but a non-thermal quasi-particle density n^* , which is conserved for the duration it takes to generate quasi-particles from the condensate, τ_g .

To compute the steady state achieved during τ_g , we

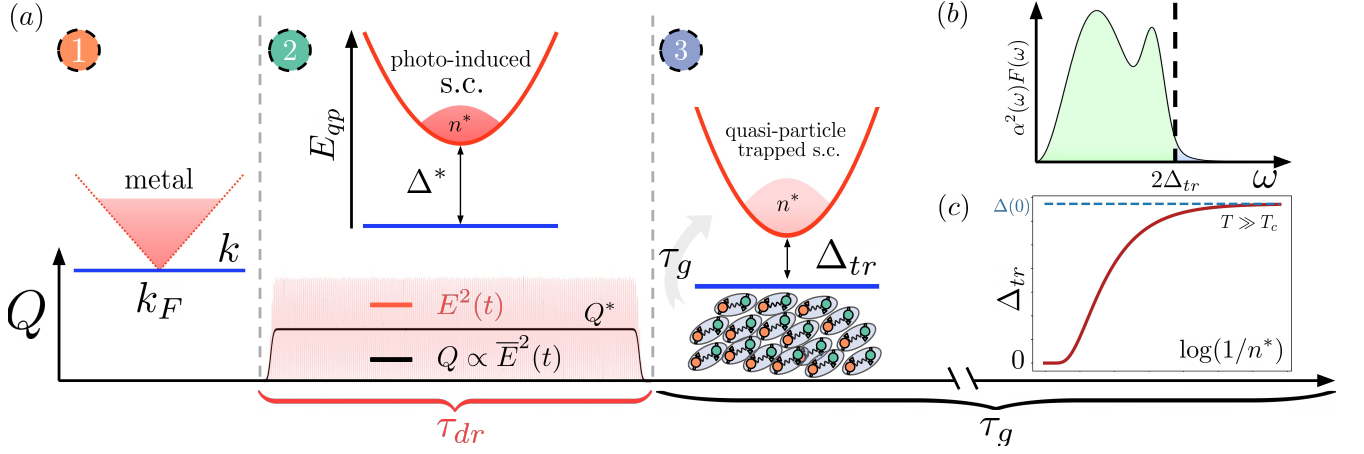


FIG. 4. **Quasi-particle Trapping** (a) Schematic for the “quasi-particle” trapping mechanism for long-lived superconductivity. Starting from the metallic phase (1), displacively driving the phonon coordinate Q from 0 to Q^* and holding it there photo-induces a superconductor with a gap Δ^* and quasi-particle density n^* (2), less than the thermal quasi-particle density in the metal. After driving for τ_{dr} , the drive is switched off and the phonon relaxes to $Q = 0$ (3). However, due to equilibration bottlenecks, the quasi-particle density n^* is frozen for a (long) duration τ_g , leading to a non-thermal state with gap Δ_{tr} . (b) Schematic of the electron-phonon spectral density $\alpha^2(\omega)F(\omega)$. While the scattering time takes into account the entire $\alpha^2(\omega)F(\omega)$ (light green and blue), the generation time τ_g depends only on $\alpha^2(\omega)F(\omega)$ for $\omega \geq 2\Delta_{tr}$. Here we show schematically a situation where the gap can lie in a frequency region with negligible electron-phonon spectral weight leading to long t_g . (c) Δ_{tr} as a function of the number of frozen quasi-particle n^* found from the solution of the superconducting gap equation under the constraint of fixed quasi-particle number. Deeper quenches (smaller n^*) lead to larger trapped gaps, until saturation to the zero-temperature gap (dashed blue) for the pairing strength at $Q = 0$.

assume that the quasi-particles population takes a non-thermal distribution which minimizes BCS free energy at temperature T , under the constraint of fixed quasi-particle density n^* . This is achieved through a Lagrange multiplier λ which acts as a “Bogolyubov chemical potential”³⁵. A fixed temperature T is maintained in the “quasi-particle band” through fast, but crucially, number-conserving scattering events with a scattering rate t_s^{-1} . We minimize the free-energy density

$$\mathcal{F}(\Delta_{tr}, \lambda) = \frac{\Delta_{tr}^2}{U_0} - 2\nu(0) \int_0^\omega d\xi \left(\sqrt{\xi^2 + \Delta_{tr}^2} - \xi \right) - 4\nu(0)T \int_0^\omega d\xi \ln \left(1 + e^{-\beta(\sqrt{\xi^2 + \Delta_{tr}^2} + \lambda)} \right) - \lambda n^*, \quad (9)$$

by finding optimal λ and Δ_{tr} . By doing so, we obtain a modified gap equation that involves a non-equilibrium quasi-particle distribution parametrized by λ , similar to the Eliashberg effect³⁶, developed to conceptualize the enhancement of T_c in microwave driven superconducting micro-bridge experiments^{37,38}:

$$\frac{1}{\nu(0)U_0} = \int_0^\omega d\xi \frac{1}{\sqrt{\xi^2 + \Delta_{tr}^2}} \tanh \left(\frac{\sqrt{\xi^2 + \Delta_{tr}^2} + \lambda}{2T} \right). \quad (10)$$

We find λ and Δ_{tr} by simultaneously solving the modified gap equation while maintaining the fixed quasi-particle

density constraint:

$$n^* = 4\nu(0) \int_0^\omega d\xi \frac{1}{\exp \left(\beta(\sqrt{\xi^2 + \Delta_{tr}^2} + \lambda) \right) + 1}. \quad (11)$$

Note that for large λ (small n^*), Eq. 10 reduces to the BCS equation at $T = 0$. Therefore, $\Delta_{tr} \rightarrow \Delta(U_0, T = 0)$ as $n^* \rightarrow 0$: larger displacive shifts Q^* induce larger Δ_{tr} , saturating at Δ_0 , the gap at $T = 0$ for a system with attractive interaction U_0 (see Fig. 4). The transient state lives for a lifetime τ_g which we compute self-consistently within Fermi’s Golden Rule³⁵, assuming that phonon induced pair-breaking is the dominant pathway for generating quasi-particles. For clarity, we quote τ_g in the limit of small n^* and low T :

$$\tau_g = \tau_0 \left(\frac{2\Delta_0}{T} \right)^{1/2} e^{-\frac{2\Delta_0}{T}} \quad (12)$$

$$\tau_0^{-1} = \frac{2}{\hbar} \pi^{\frac{3}{2}} \alpha^2(2\Delta_0) F(2\Delta_0) \quad (13)$$

Here τ_0 depends on the electron-phonon spectral density $\alpha^2(\omega)F(\omega)$ —an electron-phonon matrix element squared weighted phonon density of states³⁵—near $2\Delta_0$. τ_g can become large because the generation of quasi-particles out of the condensate necessitates the *absorption* of phonons with energy of at least $2\Delta_0$. The first consequence of this is the exponential suppression of the rate due to a lack of thermally populated low-energy phonons at $2\Delta_0$. The second consequence is that the

electron-phonon spectrum $\alpha^2(\omega)F(\omega)$ can become sparse at $\omega = 2\Delta_0$. As a result, while typical values of τ_0 can already be as long as $\sim 1ns$, for superconductivity in Zn and Al, τ_0 can reach fractions of $1\mu s$ ^{39,40}. In contrast, scattering without changing quasi-particle density involves arbitrarily low frequency acoustic phonons: accordingly, the scattering time τ_s ³⁵ involves the full $\alpha^2(\omega)F(\omega)$ and encounters no activated bottlenecks. Finally, while generating quasi-particles through phonon scattering is slow, recombining quasi-particles is not similarly bottlenecked³⁵. This implies that a long-lived superconductor can be generated by a much shorter pulse, as seen in the K_3C_{60} experiments^{11,12}.

We conclude this section by commenting on the activated enhancement of τ_g , over τ_0 , above T_c . Within weak-coupling, the activated enhancement is, at best, $\frac{\tau_g}{\tau_0} \leq \left(\frac{2\Delta_0}{T_c}\right)^{1/2} \exp\left(\frac{2\Delta_0}{T_c}\right) = 45.9$, as $\frac{2\Delta_0}{T_c} = 3.54$ within BCS. This suggests that for weak-coupling superconductors, a long photo-induced lifetime—particularly for $T \gtrsim T_c$ —necessitates a large τ_0 . This bound can be escaped by driving superconductors in which T_c is set by phase-disordering⁴¹, with a pseudo-gap region above T_c up to $T^* \gg T_c$ ⁴². For this class of superconductors, as T_c is not the scale at which the quasi-particle gap is destroyed, the activated enhancement of τ_g persists to much larger temperatures above T_c . We emphasize, however, that while a non-equilibrium (pseudo-)gap may be photo-induced for a large τ_g , our paradigm does not, on its own, generate coherence between phase-disordered Cooper pairs. Thus, while experimental signatures of a pairing gap—as reflected in e.g. optical conductivity—may be present over τ_g , phenomena relying on long-range coherence between pairs may not be seen: in the “preformed pairs” regime, our mechanism alone, does not predict a photo-induced Meissner effect.

DISCUSSION: EXPERIMENTS IN K_3C_{60} & BEYOND

Having outlined a microscopic model and two paradigms for long-lived superconductivity, we explore the implications to experiments performed in K_3C_{60} for each paradigm and comment on qualitative aspects that can be used to screen for candidate materials.

Photo-Induced Metastability

In the Supplement³⁵, we detail the mapping between our model and K_3C_{60} . In particular, we map the two band model to the t_{1u} bands of K_3C_{60} shown in Fig. 1(b) and the phonon mode to strongly coupled, inter-orbital Jahn-Teller Hg modes. While the bare parameters obtained from DFT (top, left star in Fig. 2b) lie out-

side the metastability region, strong correlations—arising from the proximity of K_3C_{60} in equilibrium to Mott insulator phase—can significantly quench the electron kinetic energy, renormalizing the electronic bandwidth, and thereby the density of states $\nu(0)$ and the effective band splitting ΔE of the t_{1u} modes. In Fig. 2b, starting from the DFT parameters, we trace a curve (white with gold stars), from a quasi-particle residue of $Z = 1$ to $Z = \frac{1}{7}$. We find that at $Z^{-1} \sim 3.5$, metastability becomes possible. Thus, accounting for the Mott renormalization of the band structure, photo-distorting specifically the Hg(3) Raman mode in K_3C_{60} offers a plausible route to light-induced metastable superconductivity in the material.

A distinct signature for metastability is the presence of Jahn-Teller static distortion that we predict in the metastable phase. Given the pico-meter scale of such a distortion, we expect that it can be detected in ultra-fast, time-resolved diffraction experiments in sufficiently clean systems. In the case where metastability II occurs, our theory predicts that metastability is a consequence of a first order phase transition already present in equilibrium due to the presence of two competing free energy minima. We note that the possibility of a first-order superconducting phase transition cannot be definitively ruled out from current experimental data⁴³, especially considering that the sharpest signatures of a first-order transition may be smeared out by spatial inhomogeneities of T_c . Uncovering experimental evidence that the transition in K_3C_{60} in equilibrium is first order could strongly fortify the metastability II scenario.

We note in passing that DMFT predictions for Cs_3C_{60} , under GPa scale pressure, place it closer to the Mott transition than K_3C_{60} . This would imply narrower bands and higher density of states, suggesting that Cs_3C_{60} crystals are a more likely candidate for the exploration of metastable superconductivity. Such a possibility underscores the fact that to realize metastable superconductivity within our microscopic paradigm, a material must simultaneously host strongly coupled, photo-distortable optical phonons and narrow bands. The unique blend of Mott, molecular, and Jahn-Teller physics present in alkali-doped fullerenes make it a paradigmatic example of a class of materials that meet such demands.

Quasi-Particle Trapping

We next turn our attention to the quasi-particle trapping mechanism, where we present strong evidence that suggests that for the trapped state, τ_0 will be large. We first highlight the consistency between the gap naively extracted from the optical conductivity, which places the “metastable” superconducting $2\Delta_{tr} \sim 8 - 12$ meV¹¹, and existing experimental characterizations of $2\Delta_0$ ^{44,45}, the maximal gap that can be attained via quasi-particle

trapping. Second, more emphatically, neutron scattering experiments⁴⁶ find a precipitous drop in the phonon density of states starting at 6 meV, persisting to 28 meV. Moreover, electron-phonon spectral density functions computed from the inversion of reflectance data^{46,47} reveal that $\alpha^2(\omega)F(\omega)$ is negligible in the vicinity of 10 – 33 meV. While more detailed single electron tunneling experiments should be performed to crisply interrogate the dissipative character of $\alpha^2(\omega)F(\omega)$ at low frequencies, the calculations based on reflectance data are consistent with the qualitative analysis of the electron-phonon coupling of the phonons at the relevant energy ranges. A long-lived superconducting $2\Delta_{tr} \sim 8 - 12$ meV would lie in a gap in the phonon spectrum between lattice modes involving octahedral K, terminating at 6.2 meV, and lattice modes involving tetrahedral K, starting at 16 meV. These phonons couple weakly to the electrons due to efficient metallic screening³¹: The next, non-negligibly coupled phonons are the Hg(1) modes at 33 meV, consistent with the reflectance data. Thus, present estimates of the electron-phonon spectral density strongly suggest that τ_0 is large, supporting a quasi-particle trapped explanation for long-lived superconductivity in K_3C_{60} .

We conclude this section with two remarks. First, we note that candidate materials for long-lived light-induced superconductivity via quasi-particle trapping can be screened by looking for superconductors in which $2\Delta_0$ lies outside the range where $\alpha^2(\omega)F(\omega)$. Second, we note that while the quantitative interrogation of the plausibility of photo-induced metastability was specific to our microscopic model, the considerations we make in the quasi-particle trapping scenario are much more generic. Indeed, this framework can be applied to any model in which the pairing attraction is photo-enhanced as the function of a laser-driven, control parameter.

Photo-Induced Resonances

The original experiments uncovering metastable photo-induced superconductivity in K_3C_{60} ¹¹ were performed around 41 THz. As the strongest coupled Jahn-Teller modes in K_3C_{60} are at much lower frequencies—13.1 THz and 22 THz frequencies for the Hg(2) and Hg(3) modes, respectively—displacively shifting these modes, thereby transiently photo-enhancing the pairing interaction, is an experimentally plausible microscopic driving mechanism. Recently, a massive resonant enhancement of the photo-susceptibility of the superconducting optical signatures was found at 10 THz¹². Within the context of our microscopic model, displacively shifting the Hg(2) mode by, e.g., non-linearly phononic interaction with the resonantly driven, IR-active (in K_3C_{60}) $T_{3u}(1)$ mode at 10 THz, could be a viable explanation for this resonance. For this situation to arise, the $T_{3u}(1)$ mode should be considerably anharmonically coupled to the Hg(2) mode.

A compelling alternative picture is the resonant driving of the Hg(3) mode itself, which is situated at 22 THz and can be driven on resonance by a laser pulse at 11 THz. In this alternative scenario the phonon coordinate is oscillating rather than being displacively shifted. To account for an oscillating phonon, in the Supplement³⁵, we perform a two stage Schrieffer-Wolff and find that the effective attraction for oscillating phonons, has terms that could be dramatically enhanced compared to the displacive shift case by an apparent resonance factor between the band ΔE and the phonon frequency ω :

$$U = \frac{4g^4\Delta E^2 \langle Q^2 \rangle}{M\omega^2 (\Delta E^2 - \omega^2)^2}. \quad (14)$$

This apparent divergence in the induced photo-attraction when $\omega \approx \Delta E$, has been investigated in Ref⁴⁸ by the authors, where it is shown that, for an oscillating phonon, the induced attraction can indeed be dramatically enhanced. However, such a scenario would be accompanied by heating and decohering scattering which would limit electron life-times. To assess whether longevity persists in the resonantly driven phonon scenario, the competition between heating and resonantly enhanced attraction should be carefully treated on equal footing by employing a non-equilibrium field theoretic approach, the subject of forthcoming investigations.

ACKNOWLEDGEMENTS

We acknowledge stimulating discussions with E. Rowe, G. Jotzu, B. Halperin, A. Polkovnikov, S. Gopalakrishnan, A. Georges, M. Devoret, P.A. Lee, M. Eckstein, & G. Refael. S.C. is grateful for support from the NSF under Grant No. DGE-1845298 & for the hospitality of the Max Planck Institute for the Structure and Dynamics of Matter. M.H.M. would like to acknowledge the support from the Alexander von Humboldt Foundation. E.D. acknowledges support from the ARO grant “Control of Many-Body States Using Strong Coherent Light-Matter Coupling in Terahertz Cavities” and the Swiss National Science Foundation under Division II. We also acknowledge support from the European Research Council (ERC-2015-AdG694097), the Cluster of Excellence “Advanced Imaging of Matter” (AIM), Grupos Consolidados (IT1453-22), Deutsche Forschungsgemeinschaft (DFG) – SFB-925 – project 170620586, DFG – Cluster of Excellence Matter and Light for Quantum Computing (ML4Q) EXC 2004/1 – 390534769 (within the RTG 1995), DFG - 508440990, and the Max Planck-New York City Center for Non-Equilibrium Quantum Phenomena. The Flatiron Institute is a division of the Simons Foundation.

- [1] Basov, D. N., Averitt, R. D. & Hsieh, D. Towards properties on demand in quantum materials. *Nature Materials* **16**, 1077–1088 (2017). URL <https://www.nature.com/articles/nmat5017>.
- [2] de la Torre, A. *et al.* Colloquium: Nonthermal pathways to ultrafast control in quantum materials. *Reviews of Modern Physics* **93**, 041002 (2021). URL <https://link.aps.org/doi/10.1103/RevModPhys.93.041002>. Publisher: American Physical Society.
- [3] Nova, T. F., Disa, A. S., Fechner, M. & Cavalleri, A. Metastable ferroelectricity in optically strained SrTiO_3 . *Science* **364**, 1075–1079 (2019). URL <https://www.science.org/doi/abs/10.1126/science.aaw4911>. <https://www.science.org/doi/pdf/10.1126/science.aaw4911>.
- [4] Li, X. *et al.* Terahertz field-induced ferroelectricity in quantum paraelectric SrTiO_3 . *Science* **364**, 1079–1082 (2019). URL <https://www.science.org/doi/10.1126/science.aaw4913>. Publisher: American Association for the Advancement of Science.
- [5] Kogar, A. *et al.* Light-induced charge density wave in LaTe_3 . *Nature Physics* **16**, 159–163 (2020). URL <https://doi.org/10.1038/s41567-019-0705-3>.
- [6] Dolgirev, P. E., Michael, M. H., Zong, A., Gedik, N. & Demler, E. Self-similar dynamics of order parameter fluctuations in pump-probe experiments. *Phys. Rev. B* **101**, 174306 (2020). URL <https://link.aps.org/doi/10.1103/PhysRevB.101.174306>.
- [7] Disa, A. S. *et al.* Optical stabilization of fluctuating high temperature ferromagnetism in ytio_3 (2021). URL <https://arxiv.org/abs/2111.13622>.
- [8] von Hoegen, A. *et al.* Amplification of superconducting fluctuations in driven $\text{YBa}_2\text{Cu}_3\text{O}_6$. *Phys. Rev. X* **12**, 031008 (2022). URL <https://link.aps.org/doi/10.1103/PhysRevX.12.031008>.
- [9] Michael, M. H. *et al.* Parametric resonance of Josephson plasma waves: A theory for optically amplified interlayer superconductivity in $\text{YBa}_2\text{Cu}_3\text{O}_6$. *Phys. Rev. B* **102**, 174505 (2020). URL <https://link.aps.org/doi/10.1103/PhysRevB.102.174505>.
- [10] Mitrano, M. *et al.* Possible light-induced superconductivity in k3c60 at high temperature. *Nature* **530**, 461–464 (2016). URL <https://doi.org/10.1038/nature16522>.
- [11] Budden, M. *et al.* Evidence for metastable photo-induced superconductivity in K_3C_{60} . *Nature Physics* **17**, 611–618 (2021). URL <https://doi.org/10.1038/s41567-020-01148-1>.
- [12] Rowe, E. *et al.* Giant resonant enhancement for photo-induced superconductivity in K_3C_{60} (2023). URL <https://arxiv.org/abs/2301.08633>.
- [13] Kennes, D. M., Wilner, E. Y., Reichman, D. R. & Millis, A. J. Transient superconductivity from electronic squeezing of optically pumped phonons. *Nature Phys* **13**, 479–483 (2017). URL <https://www.nature.com/articles/nphys4024>. Number: 5 Publisher: Nature Publishing Group.
- [14] Komnik, A. & Thorwart, M. BCS theory of driven superconductivity. *Eur. Phys. J. B* **89**, 244 (2016). URL <https://doi.org/10.1140/epjb/e2016-70528-1>.
- [15] Nava, A., Giannetti, C., Georges, A., Tosatti, E. & Fabrizio, M. Cooling quasiparticles in A3C60 fullerenes by excitonic mid-infrared absorption. *Nat. Phys.* **14**, 154–159 (2018). URL <https://www.nature.com/articles/nphys4288>. Number: 2 Publisher: Nature Publishing Group.
- [16] Knap, M., Babadi, M., Refael, G., Martin, I. & Demler, E. Dynamical Cooper pairing in nonequilibrium electron-phonon systems. *Phys. Rev. B* **94**, 214504 (2016). URL <https://link.aps.org/doi/10.1103/PhysRevB.94.214504>. Publisher: American Physical Society.
- [17] Raines, Z. M., Stanev, V. & Galitski, V. M. Enhancement of superconductivity via periodic modulation in a three-dimensional model of cuprates. *Phys. Rev. B* **91**, 184506 (2015). URL <https://link.aps.org/doi/10.1103/PhysRevB.91.184506>. Publisher: American Physical Society.
- [18] Coulthard, J. R., Clark, S. R., Al-Assam, S., Cavalleri, A. & Jaksch, D. Enhancement of superexchange pairing in the periodically driven Hubbard model. *Phys. Rev. B* **96**, 085104 (2017). URL <https://link.aps.org/doi/10.1103/PhysRevB.96.085104>. Publisher: American Physical Society.
- [19] Kim, M. *et al.* Enhancing superconductivity in A_3C_{60} fullerides. *Phys. Rev. B* **94**, 155152 (2016). URL <https://link.aps.org/doi/10.1103/PhysRevB.94.155152>. Publisher: American Physical Society.
- [20] Sentef, M. A. Light-enhanced electron-phonon coupling from nonlinear electron-phonon coupling. *Phys. Rev. B* **95**, 205111 (2017). URL <https://link.aps.org/doi/10.1103/PhysRevB.95.205111>. Publisher: American Physical Society.
- [21] Sentef, M. A., Kemper, A. F., Georges, A. & Kollath, C. Theory of light-enhanced phonon-mediated superconductivity. *Phys. Rev. B* **93**, 144506 (2016). URL <https://link.aps.org/doi/10.1103/PhysRevB.93.144506>. Publisher: American Physical Society.
- [22] Michael, M. H. *et al.* Parametric resonance of Josephson plasma waves: A theory for optically amplified interlayer superconductivity in YBaCu_3O_6 . *Phys. Rev. B* **102**, 174505 (2020). URL <https://link.aps.org/doi/10.1103/PhysRevB.102.174505>. Publisher: American Physical Society.
- [23] Denny, S., Clark, S., Laplace, Y., Cavalleri, A. & Jaksch, D. Proposed Parametric Cooling of Bilayer Cuprate Superconductors by Terahertz Excitation. *Phys. Rev. Lett.* **114**, 137001 (2015). URL <https://link.aps.org/doi/10.1103/PhysRevLett.114.137001>. Publisher: American Physical Society.
- [24] Okamoto, J.-i., Cavalleri, A. & Mathey, L. Theory of Enhanced Interlayer Tunneling in Optically Driven High- T_c Superconductors. *Phys. Rev. Lett.* **117**, 227001 (2016). URL <https://link.aps.org/doi/10.1103/PhysRevLett.117.227001>. Publisher: American Physical Society.
- [25] Dolgirev, P. E. *et al.* Periodic dynamics in superconductors induced by an impulsive optical quench. *Commun Phys* **5**, 1–9 (2022). URL <https://www.nature.com/articles/s42005-022-01007-w>. Number: 1 Publisher: Nature Publishing Group.
- [26] Babadi, M., Knap, M., Martin, I., Refael, G. & Demler, E. Theory of parametrically amplified electron-phonon superconductivity. *Phys. Rev. B* **96**, 014512 (2017). URL <https://link.aps.org/doi/10.1103/PhysRevB.96.014512>. Publisher: American Physical Society.

- ciety.
- [27] Dasari, N. & Eckstein, M. Transient Floquet engineering of superconductivity. *Phys. Rev. B* **98**, 235149 (2018). URL <https://link.aps.org/doi/10.1103/PhysRevB.98.235149>. Publisher: American Physical Society.
- [28] Mazza, G. & Georges, A. Nonequilibrium superconductivity in driven alkali-doped fullerides. *Phys. Rev. B* **96**, 064515 (2017). URL <https://link.aps.org/doi/10.1103/PhysRevB.96.064515>. Publisher: American Physical Society.
- [29] Dai, Z. & Lee, P. A. Superconducting-like response in driven systems near the Mott transition. *Phys. Rev. B* **104**, L241112 (2021). URL <https://link.aps.org/doi/10.1103/PhysRevB.104.L241112>. Publisher: American Physical Society.
- [30] van der Marel, D., Barantani, F. & Rischau, C. W. Possible mechanism for superconductivity in doped srtio₃. *Phys. Rev. Res.* **1**, 013003 (2019). URL <https://link.aps.org/doi/10.1103/PhysRevResearch.1.013003>.
- [31] Gunnarsson, O. *Alkali-Doped Fullerides* (WORLD SCIENTIFIC, 2004). URL <https://www.worldscientific.com/doi/abs/10.1142/5404>. <https://www.worldscientific.com/doi/pdf/10.1142/5404>.
- [32] Först, M. *et al.* Nonlinear phonics as an ultrafast route to lattice control. *Nature Physics* **7**, 854–856 (2011). URL <https://doi.org/10.1038/nphys2055>.
- [33] Suhl, H., Matthias, B. T. & Walker, L. R. Bardeen-cooper-schrieffer theory of superconductivity in the case of overlapping bands. *Phys. Rev. Lett.* **3**, 552–554 (1959). URL <https://link.aps.org/doi/10.1103/PhysRevLett.3.552>.
- [34] Kondo, J. Superconductivity in Transition Metals. *Progress of Theoretical Physics* **29**, 1–9 (1963). URL <https://doi.org/10.1143/PTP.29.1>.
- [35] See Supplementary Material.
- [36] Eliashberg, G. M. Film superconductivity stimulated by a high-frequency field. *JETP Lett. (USSR) (Engl. Transl.); (United States)* **11** (1970). URL <https://www.osti.gov/biblio/7361235>.
- [37] Wyatt, A. F. G., Dmitriev, V. M., Moore, W. S. & Sheard, F. W. Microwave-enhanced critical supercurrents in constricted tin films. *Phys. Rev. Lett.* **16**, 1166–1169 (1966). URL <https://link.aps.org/doi/10.1103/PhysRevLett.16.1166>.
- [38] Dayem, A. H. & Wiegand, J. J. Behavior of thin-film superconducting bridges in a microwave field. *Phys. Rev.* **155**, 419–428 (1967). URL <https://link.aps.org/doi/10.1103/PhysRev.155.419>.
- [39] Kaplan, S. B. *et al.* Quasiparticle and phonon lifetimes in superconductors. *Phys. Rev. B* **14**, 4854–4873 (1976). URL <https://link.aps.org/doi/10.1103/PhysRevB.14.4854>.
- [40] Levine, J. L. & Hsieh, S. Y. Recombination time of quasiparticles in superconducting aluminum. *Phys. Rev. Lett.* **20**, 994–997 (1968). URL <https://link.aps.org/doi/10.1103/PhysRevLett.20.994>.
- [41] Emery, V. J. & Kivelson, S. A. Importance of phase fluctuations in superconductors with small superfluid density. *Nature* **374**, 434–437 (1995). URL <https://doi.org/10.1038/374434a0>.
- [42] Indeed, there is a panoply of experimental evidence in K₃C₆₀ that suggests deviations from weak coupling theory, from anomalously large values of $\frac{2\Delta_0}{T_c} \sim 5.3$ in bulk and ~ 6.5 in thin-films^{44,45}, to a recently uncovered psuedo-gap in thin films⁴⁵, to the lattice-spacing scale coherence length of Cooper pairs³¹, to anomalous Nernst signals persisting up to 80K⁴⁹.
- [43] Ramirez, A. P., Rosseinsky, M. J., Murphy, D. W. & Haddon, R. C. Specific-heat jump at t_c and normal-state magnetic susceptibility of A₃C₆₀. *Phys. Rev. Lett.* **69**, 1687–1690 (1992). URL <https://link.aps.org/doi/10.1103/PhysRevLett.69.1687>.
- [44] Zhang, Z., Chen, C.-C. & Lieber, C. M. Tunneling spectroscopy of M₃C₆₀ superconductors: The energy gap, strong coupling, and superconductivity. *Science* **254**, 1619–1621 (1991). URL <https://www.science.org/doi/abs/10.1126/science.254.5038.1619>. <https://www.science.org/doi/pdf/10.1126>.
- [45] Ren, M.-Q. *et al.* Direct observation of full-gap superconductivity and pseudogap in two-dimensional fullerides. *Phys. Rev. Lett.* **124**, 187001 (2020). URL <https://link.aps.org/doi/10.1103/PhysRevLett.124.187001>.
- [46] Pintschovius, L. Neutron studies of vibrations in fullerenes. *Reports on Progress in Physics* **59**, 473 (1996). URL <https://dx.doi.org/10.1088/0034-4885/59/4/001>.
- [47] Degiorgi, L. *et al.* Optical properties of the alkali-metal-doped superconducting fullerenes: K₃C₆₀ and Rb₃C₆₀. *Phys. Rev. B* **49**, 7012–7025 (1994). URL <https://link.aps.org/doi/10.1103/PhysRevB.49.7012>.
- [48] Eckhardt, C. J. *et al.* Theory of resonantly enhanced photo-induced superconductivity (2023). URL <http://arxiv.org/abs/2303.02176>. ArXiv:2303.02176.
- [49] Jotzu, G. *et al.* Superconducting fluctuations observed far above t_c in the isotropic superconductor K₃C₆₀ (2021). URL <https://arxiv.org/abs/2109.08679>.
- [50] Schrieffer, J. R. *Theory of superconductivity*.
- [51] Rothwarf, A. & Taylor, B. N. Measurement of recombination lifetimes in superconductors. *Phys. Rev. Lett.* **19**, 27–30 (1967). URL <https://link.aps.org/doi/10.1103/PhysRevLett.19.27>.
- [52] Nomura, Y., Sakai, S., Capone, M. & Arita, R. Unified understanding of superconductivity and mott transition in alkali-doped fullerides from first principles. *Science Advances* **1**, e1500568 (2015). URL <https://www.science.org/doi/abs/10.1126/sciadv.1500568>. <https://www.science.org/doi/pdf/10.1126/sciadv.1500568>.
- [53] Rice, M. J., Choi, H. Y. & Wang, Y. R. Three-band superconductivity in K₃C₆₀ and Rb₃C₆₀. *Phys. Rev. B* **44**, 10414–10416 (1991). URL <https://link.aps.org/doi/10.1103/PhysRevB.44.10414>.
- [54] Iwahara, N., Sato, T., Tanaka, K. & Chibotaru, L. F. Vibronic coupling in C₆₀ anion revisited: Derivations from photoelectron spectra and dft calculations. *Phys. Rev. B* **82**, 245409 (2010). URL <https://link.aps.org/doi/10.1103/PhysRevB.82.245409>.
- [55] Michael, M. *et al.* Fresnel-floquet theory of light-induced terahertz reflectivity amplification in Ta₂NiSe₅ (2022). URL <https://arxiv.org/abs/2207.08851>.

Supplementary Materials

Appendix A: $\langle Q \rangle$ -dependent superconductivity through a Raman displacive shift

In this Appendix, using a local electron-phonon coupling model, we derive an s -wave pairing interaction by performing a judiciously chosen rotation and a Schrieffer-Wolff transformation on a simple, local model to obtain a non-trivial, $\langle Q \rangle$ dependent pairing strength. We start with an effective Hamiltonian given by two levels separated by a splitting ΔE and an Einstein phonon that couples to transition between the two levels:

$$H = \sum_i \left(-\Delta E S_i^z + 2gQ_i S_i^x + \frac{P_i^2}{2M} + \frac{M\omega^2}{2} Q_i^2 \right). \quad (\text{A1})$$

In equation (A1), the spin-operators are given by, $S_i^z = \frac{1}{2} \sum_\sigma (c_{i,\sigma}^\dagger c_{i,\sigma} - d_{i,\sigma}^\dagger d_{i,\sigma})$ and $S_i^x = \frac{1}{2} \sum_\sigma (c_{i,\sigma}^\dagger d_{i,\sigma} + d_{i,\sigma}^\dagger c_{i,\sigma})$ in terms of the Fermion operator c, d for the two local electronic states and where $\sigma \in \{\uparrow, \downarrow\}$ are the usual spin-indices. Since we concern ourselves with a homogenized system and local physics in the ensuing, we drop the space index for the remainder of the derivation. In the presence of a fixed distortion $\langle Q \rangle$, we re-write $Q = \langle Q \rangle + \tilde{Q}$, where \tilde{Q} are the fluctuations in the phonon coordinate. Our aim is to move into the diagonal basis of the electronic Hamiltonian given by the splitting of the levels and the mean coordinate $\langle Q \rangle - H_{el}(\langle Q \rangle) = -\Delta E S^z + 2g \langle Q \rangle S_i^x$ —in order to account for distortion induced hybridization between the c and d levels to all orders in $\langle Q \rangle$. Specifically we perform the following rotation:

$$\begin{pmatrix} \tilde{c} \\ \tilde{d} \end{pmatrix} = \begin{pmatrix} \cos(\theta) & \sin(\theta) \\ -\sin(\theta) & \cos(\theta) \end{pmatrix} \begin{pmatrix} c \\ d \end{pmatrix}, \quad (\text{A2})$$

where θ is given by $\tan(2\theta) = \frac{2g\langle Q \rangle}{\Delta E}$. We now write our Hamiltonian as $H = H_0 + H_{el-ph}$. The free Hamiltonian $H_0 = -\Delta_{eff} \tilde{S}^z + \frac{P^2}{2M} + \frac{M\omega^2}{2} Q^2$, where $\Delta_{eff} = \sqrt{\Delta E^2 + (2g\langle Q \rangle)^2}$.

The effective electron-phonon interaction in the rotated basis becomes:

$$H_{el-ph} = 2g \sin(2\theta) \tilde{Q} \tilde{S}^z + 2g \cos(2\theta) \tilde{Q} \tilde{S}^x, \quad (\text{A3})$$

where the hybridization of the original two-levels leads to a term that couples the fluctuations of the phonon coordinate directly to the density, as in the Hubbard-Holstein model.

We proceed by handling the interaction Hamiltonian perturbatively in g by performing a Schrieffer-Wolff transformation that removes the electron-phonon interaction to linear order. In particular, we use the following unitary:

$$U_{SW} = e^{i(\alpha_x \tilde{S}^x \tilde{P} + \alpha_z \tilde{S}^z \tilde{P} + \beta_y \tilde{S}^y \tilde{Q})}. \quad (\text{A4})$$

where $\alpha_x = \frac{2g \cos(2\theta)}{M(\Delta_{eff}^2 - \omega^2)}$, $\alpha_z = -\frac{2g \sin(2\theta)}{M\omega^2}$, $\beta_y = \frac{2g \cos(2\theta)}{\Delta_{eff}^2 - \omega^2} \Delta_{eff}$.

To lowest non-trivial order in g , the final electronic Hamiltonian takes the form:

$$H_{el} = -\Delta_{eff} \tilde{S}_z + U_z \tilde{S}_z^2 + U_x \tilde{S}_x^2. \quad (\text{A5})$$

Both U_z and U_x contain anomalous, BCS-type contributions and a comprehensive treatment of the problem would require considering the multi-band superconductivity that arises from the interplay between these two terms (near the regime in which the level splitting and the phonon frequency are resonant, this factor must be considered carefully (see Ref.⁴⁸). However, in the limit that the gap Δ_{eff} is large, the upper, \tilde{d} -levels are occupied only virtually. Therefore, fixing our attention on solely the lower c -electrons, expanding the \tilde{S}_z^2 term, and retaining only anomalous contributions, we arrive at the following $\langle Q \rangle$ dependent, on-site, *attractive* interaction:

$$H_{int,i} = -\frac{g^2}{M\omega^2} \frac{4g^2 \langle Q \rangle^2}{\Delta E^2 + 4g^2 \langle Q \rangle^2} \tilde{c}_{i,\uparrow}^\dagger \tilde{c}_{i,\downarrow}^\dagger \tilde{c}_{i,\uparrow} \tilde{c}_{i,\downarrow} \quad (\text{A6})$$

We now make two comments on the extension of this derivation in the local limit to include the hopping. The first is that, the term $2g \sin(2\theta) \tilde{Q} \tilde{S}^z = 2g'(\langle Q \rangle) \tilde{Q} \tilde{S}^z$ in equation (A3) couples the phonon coordinate directly to the electron density, as in the Holstein model. We focus on this term, ignoring the $\tilde{Q} \tilde{S}^x$ term which induces inter-band pairing that is irrelevant away from the resonance between the phonon and the level splitting ΔE .

Our second comment concerns the interplay between our rotation and Schrieffer-Wolff transformation and the hopping. As we choose the hopping for both c and d electrons the same, the rotation has no effect. The Schrieffer-Wolff transformation, however, does introduce extra hopping between levels. An estimate for when these new terms can be ignored is found by comparing their magnitude— $\frac{g\ell_0}{\Delta_{eff}} t$, where t is hopping strength and ℓ_0 is the oscillator length of the phonons—to the scale of the interaction—set by the saturation value of $\frac{g^2}{M\omega^2}$. This implies that our local considerations should not invite concern as long as $\frac{t\omega}{\Delta_{eff}} \ll g\ell_0$. This condition should hold forth in the context of experiments performed in alkali-doped fullerenes, where the proximity of the system to a Mott-phase further narrows bands which are already thin due to the significant distances that electrons have to hop in the C_{60} molecule.

Appendix B: Thermodynamics with fixed quasi-particle number

In this section we provide a derivation of the steady state equations Eqs. 9-11 within the BCS mean field approximation. We begin by reiterating that (number conserving) scattering between quasi-particles and thermally occupied acoustic phonons is much faster than number non-conserving scattering events needed to generate quasi-particles. While the latter is emphasized throughout our work as what enables a long-lived non-equilibrium gap, the former suggests that the effective temperature that governs the quasi-particle distribution should coincide with the temperature of the phonon bath. Thus, to find our steady state quasi-particle distribution, it suffices to solve for the gap Δ and Bogolyubov chemical potential λ self-consistently while minimizing an effective thermal free energy at temperature T . Concretely, our quasi-particle number constrained, Δ -dependent free energy can be expressed as:

$$F(\Delta) = \text{Tr}\{\rho H(\Delta)\} + T \text{Tr}\{\rho \log \rho\} + \lambda \left(\text{Tr}\left\{\rho \sum_{k,\sigma} \gamma_{k,\sigma}^\dagger(\Delta) \gamma_{k,\sigma}(\Delta)\right\} - n^* \right) + z (\text{Tr}\{\rho\} - 1), \quad (\text{B1})$$

where the first two terms correspond to the usual BCS decoupled free energy at a given temperature and superconducting gap Δ , the fixed quasi-particle constraint is enforced by minimizing with respect to a Lagrange multiplier λ , and the final term enforces that the density matrix has trace 1, by minimizing with respect to z . The operators $\gamma_{k,\sigma}(\Delta)$ ($\gamma_{k,\sigma}^\dagger(\Delta)$) correspond to the Bogolyubov quasi-particle annihilation (creation) operators defined by canonical Bogolyubov rotations parametrized by Δ : $\gamma_{k,\uparrow} = u_k c_{k,\uparrow} - v_k c_{k,\downarrow}^\dagger$ and $\gamma_{-k,\downarrow}^\dagger = u_k^* c_{-k,\downarrow}^\dagger - v_k^* c_{k,\uparrow}$, where $|u_k|^2 = \frac{1}{2} \left(1 + \frac{\xi_k}{\sqrt{\xi_k^2 + \Delta^2}} \right)$ and $|v_k|^2 + |u_k|^2 = 1$. We note now that the operator portion of the quasi-particle number constraint can be subsumed into the Hamiltonian, which within BCS mean-field, is diagonal in $\gamma_{k,\sigma}(\Delta)$. Thus, one readily interprets the Lagrange multiplier as a chemical potential for the Bogolyubov quasi-particles.

For completeness, by factorizing our density matrix into different momentum k -dependent and pseudo-spin σ -dependent contributions,

$$\rho = \prod_{k,\sigma} \rho_{k,\sigma}, \quad \text{with} \quad \text{Tr}\{\rho_{k,\sigma}\} = 1. \quad (\text{B2})$$

The $\rho_{k,\sigma}$'s are found by minimizing F :

$$\frac{\partial F}{\partial \rho_{k,\sigma}} = E_k \left\langle \gamma_{k,\sigma}^\dagger \gamma_{k,\sigma} \right\rangle + T \log(\rho_{k,\sigma}) + T + \lambda \left\langle \gamma_{k,\sigma}^\dagger \gamma_{k,\sigma} \right\rangle + z = 0, \quad (\text{B3})$$

$$\Rightarrow \rho = \frac{e^{-\beta \sum_{k,\sigma} (E_k + \lambda) \gamma_{k,\sigma}^\dagger \gamma_{k,\sigma}}}{Z_k}, \quad (\text{B4})$$

where λ and Δ are determined self-consistently as:

$$n^* = \sum_{k,\sigma} \left\langle \gamma_{k,\sigma}^\dagger \gamma_{k,\sigma} \right\rangle = \sum_{k,\sigma} \frac{1}{\exp\left(\beta(\sqrt{\xi_k^2 + \Delta^2} + \lambda)\right) + 1} \quad (\text{B5})$$

$$\Delta = \frac{U}{N} \sum_{\substack{k \\ |\xi_k| < \omega}} \langle c_{-k,\downarrow} c_{k,\uparrow} \rangle = \frac{U}{N} \sum_{\substack{k \\ |\xi_k| < \omega}} u_k^* v_k (1 - 2 \langle \gamma_{k,\uparrow}^\dagger \gamma_{k,\uparrow} \rangle) = \frac{U}{N} \sum_{\substack{k \\ |\xi_k| < \omega}} \frac{\Delta}{2\sqrt{\xi_k^2 + \Delta^2}} \tanh\left(\beta(\sqrt{\xi_k^2 + \Delta^2} + \lambda)\right) \quad (\text{B6})$$

Appendix C: Quasi-particle equilibration time-scales

In this section we derive a set of characteristic time-scales relevant to the equilibration of Bogolyubov quasi-particles coupled to a thermal bath of phonons. We note that these phonons are low-energy and are weakly-coupled to the electrons—despite this, they are thermally occupied at the temperatures we consider. We assume that the primary function of these low energy phonons is dissipative while higher energy optical phonons are responsible for the pairing glue. This is the case in K_3C_{60} where, as a reminder, neutron scattering data⁴⁶ shows significant density of states due to acoustic and librational phonons up to 6 meV, a significant drop off in the phonon spectrum between 10-33 meV (a regime dominated by weakly coupled potassium lattice modes), and then phonons corresponding to on ball molecular vibrations starting with the Hg(1) mode at 33 meV.

We introduce a weakly coupled bath of low-energy, phonons, with electron-phonon interactions given by:

$$H_{\text{bath}} = \sum_{p,p',\lambda,\sigma} g_{p,p',\lambda} (a_{q,\lambda} + a_{-q,\lambda}^\dagger) c_{p,s}^\dagger c_{p,\sigma} \quad (\text{C1})$$

where λ runs over the polarizations of the phonons, $g_{p,p',\lambda}$ yields a momentum and polarization dependent electron-phonon coupling, $q = p - p'$ —considering only the relevant normal processes—and $\sigma \in \{\uparrow, \downarrow\}$. Leveraging the assumption that electrons are coupled weakly to the low-lying phonons, we estimate the quasi-particle-phonon scattering times perturbatively using Fermi's Golden Rule. Along the lines of Ref.³⁹, we delineate between three different equilibration rates: (1) $\gamma_s = \frac{1}{\tau_s}$, the rate of scattering between Bogolyubov quasi-particles by the acoustic phonons *without changing the total number of quasi-particles*, (2) $\gamma_r = \frac{1}{\tau_r}$ the rate at which quasi-particles re-combine into Cooper-pairs, and an additional rate: (3) $\gamma_g = \frac{1}{\tau_g}$, the rate at which quasi-particles are generated by Cooper-pairs scattering into phonons. In the context at hand, as the interaction strength is lowered, there is a *dearth* of thermal quasi-particles, as opposed to an excess, as is the conventional non-equilibrium case when a quasi-particle current is injected. In the presence of a *lack* of thermal quasi-particles, τ_g provides a minimal time-scale for which the post-drive, fixed number of quasi-particles approximation—and the transient, possibly long-lived, superconductivity it enables—is sensible.

We compute the Fermi's golden rule rate by using H_{bath} as the perturbation and picking an initial state $|I\rangle$ sampled from a density matrix formed by the Kronecker product of a thermal density matrix of phonons at a temperature T and, for the electrons, an arbitrary quasi-particle occupation function⁵⁰. In thermal equilibrium, this is the Fermi-Dirac distribution; in the quasi-particle trapped steady state, this is given by $f(E) = \frac{1}{\exp(\beta(E+\lambda))+1}$.

In the ensuing, we focus first on process (3), the generation of quasi-particles by scattering with bath phonons. The first two processes are discussed in detail in³⁹. We simplify our discussion by computing the generation time for a fixed quasi-particle at the gap energy Δ and with momentum $k = 0$ and spin \uparrow . The process whose rate we seek to compute is one which involves the absorption of a phonon at energy Ω and the generation of two quasi-particles, one at energy Δ , the other at energy $\Omega - \Delta \geq \Delta$. We write one possible final state as $|F\rangle_{q,\lambda} = \gamma_{k,\uparrow}^\dagger \gamma_{q,\downarrow}^\dagger a_{k-q,\lambda} |I\rangle$. To compute the total scattering rate, we sum over quasi-particle momenta q .

We make progress by noting that terms such $c_{p',\uparrow}^\dagger c_{p,\uparrow} + c_{-p,\downarrow}^\dagger c_{-p',\downarrow}$ can be written in terms of Bogolyubov quasi-particle operators as: $c_{p',\uparrow}^\dagger c_{p,\uparrow} + c_{-p,\downarrow}^\dagger c_{-p',\downarrow} = t(p,p')(\gamma_{p,\uparrow}^\dagger \gamma_{p',\uparrow} + \gamma_{-p,\downarrow}^\dagger \gamma_{-p',\downarrow}) + m(p,p')(\gamma_{p',\uparrow}^\dagger \gamma_{-p,\downarrow} - \gamma_{p,\uparrow} \gamma_{-p',\downarrow})$, where $t(p,p')$ and $m(p,p')$ are the standard coherence factors: $m(p,p') = \frac{1}{2}(1 + \frac{\epsilon_p \epsilon_{p'} + \Delta^2}{E_p E_{p'}})$ and $t(p,p') = \frac{1}{2}(1 + \frac{\epsilon_p \epsilon_{p'} - \Delta^2}{E_p E_{p'}})$. Using this, we can express the square of our desired matrix elements as: $|\langle I | H_{\text{bath}} | F \rangle_{q,\lambda}|^2 = g_{k-q,\lambda}^2 m^2(k,q) (1 - \nu_{q,\downarrow})(1 - \nu_{k,\uparrow}) n_{ph}(k-q,\lambda)$, where ν_q is the occupation number of a quasi-particle at momentum q and $n_{ph}(k-q,\lambda)$ is the occupation number of a phonon at momentum $k-q$ and polarization λ in the initial state $|I\rangle$. Note that while $|I\rangle$ is a pure state, the rate will be averaged over occupation numbers given by the ensemble from which $|I\rangle$ is drawn from, as prescribed above.

Computing the sum over q in the continuum, we introduce the standard Bogolyubov density of states—for a quasi-particle at energy E , the DOS goes as $\rho(E) = \frac{E}{\sqrt{E^2 - \Delta^2}}$ —and phonon spectral density $F(\Omega)$, weighted by the square

of the matrix element $\alpha^2(\Omega)$, averaged over the Fermi surface. Specifically, borrowing notation from Ref.³⁹, we define:

$$\alpha^2(\Omega)F(\Omega) = \frac{1}{\int dp^2} \sum_{\lambda} \int dp^2 \int \frac{dp'^2}{(2\pi)^3 v_F} |g_{p-p',\lambda}|^2 \delta(\Omega - \omega_{p-p',\lambda}) \quad (\text{C2})$$

Using these definitions and our computation of the matrix element above, we arrive at our result for the rate at which quasi-particles are generated by the scattering of Cooper pairs with low-frequency phonons:

$$\Gamma_g(\Delta) = \frac{2\pi}{\hbar} \int_{2\Delta}^{\infty} d\Omega \left(\alpha^2(\Omega)F(\Omega) \sqrt{\frac{\Omega}{\Omega - 2\Delta}} (1 - f(\Omega - \Delta))(1 - f(\Delta))n(\Omega) \right) \quad (\text{C3})$$

As a reminder, as our initial density matrix is “quasi-particle trapped” and therefore, $f(E) = \frac{1}{\exp(\beta(E+\lambda))+1}$. As evident upon inspection, in the limit of large 2Δ , the rate is suppressed by the scarcity of thermal phonons at 2Δ . Moreover, it remains clear that this rate depends on $\alpha^2(\Omega)F(\Omega)$ above 2Δ .

The scattering time τ_s which controls thermal equilibration within each quasi-particle band is given by:

$$\Gamma_s(\Delta) = \frac{2\pi}{\hbar} \int_0^{\infty} d\Omega \left(\alpha^2(\Omega)F(\Omega) \sqrt{\frac{\Omega}{\Omega + 2\Delta}} (1 - f(\Delta + \Omega))(1 - f(\Delta))n(\Omega) \right), \quad (\text{C4})$$

Here, while the phonon distribution is the thermal Bose-Einstein distribution, $f(E)$ is not—generically (e.g., for the quasi-particle trapped superconductor)—a thermal Dirac distribution. Note that Γ_s can be much larger than Γ_g as low-frequency acoustic modes can be significantly thermally populated as arbitrarily low-frequency phonons can participate in number-conserving scattering processes. Moreover, this rate is sensitive to the electron-phonon spectral function at *all* frequencies, picking up not only acoustic contributions but low-lying optical ones below 2Δ . Our arguments for a fast scattering, t_s time but a very slow generation time, t_g , provide justification for our approximation that a superconducting steady state is reached described by a temperature and a conserved number of quasi-particles.

Having argued for the large discrepancy between scattering rates that thermalize the Bogolyubov quasi-particles and rates for generating new quasi-particles, we now argue that the asymmetry between quasi-particle recombination during driving and quasi-particle generation after driving implies that our long-lived superconductor can be generated by a short pulse, as seen in experiments^{11,12}. While generating quasi-particles out of the condensate can be slow due to the absence of thermally excited phonons, recombining a pair of quasi-particles requires emitting a phonon, and is therefore not bottlenecked by the phonon population. The recombination bottleneck in traditional “Rothwarf-Taylor” quasi-particle injection experiments arises instead from a dearth of thermally excited quasi-particle partners that are needed for recombining the injected quasi-particle⁵¹. This is apparent if one considers the recombination rate within Fermi’s Golden Rule:

$$\Gamma_r(\Delta) = \frac{2\pi}{\hbar} \int_{2\Delta}^{\infty} d\Omega \left(\alpha^2(\Omega)F(\Omega) \sqrt{\frac{\Omega}{\Omega - 2\Delta}} f(\Omega - \Delta)(1 - f(\Delta))(1 + n(\Omega)) \right). \quad (\text{C5})$$

We emphasize again that this rate, in general, is computed for a non-equilibrium quasi-particle distribution function $f(E)$. In the quasi-particle injection experiments $f(\Omega - \Delta) \sim e^{-\frac{\Delta}{k_B T}}$ at low-temperatures. In our context, however, if one rapidly ramps U to U^* , the recombination process is not slowed down due to a *lack* of quasi-particles: in this situation, there is not a lack but an *excess* of non-thermally distributed quasi-particles that need to be recombined. Moreover, while quasi-particle generation can be bottlenecked by a small $\alpha^2(\Delta_{tr})F(\Delta_{tr})$, it is generally true that $\Delta^* \gg \Delta$ and therefore it is possible that $\alpha^2(\Delta_{tr})F(\Delta_{tr}) \ll \alpha^2(\Delta^*)F(\Delta^*)$. This is especially possible if $\alpha^2(\Omega)F(\Omega)$ has a size-able frequency gap, as seems to be the case in K_3C_{60} . Thus, within our context, there are no clear bottlenecks for quasi-particle recombination during driving. This difference in the time-scales between recombining quasi-particles and generating quasi-particles allows us to create a superconducting state with a considerably shorter pulse than the life-time of the superconductor.

Appendix D: Mapping to K_3C_{60}

In this section we review details and literature of K_3C_{60} , in order to match our model to K_3C_{60} and derive realistic parameters. The prevailing consensus on the origin of high- T_c equilibrium, s-wave superconductivity in K_3C_{60} implicates an interplay between attraction facilitated by Jahn-Teller Hg modes that are strongly coupled to partially filled t_{1u} bands and strong electronic correlations that arise from the materials proximity to the Mott transition^{31,52}. The latter leads to a dramatic suppression of charge fluctuations and significant renormalization of both the onsite Coulomb repulsion (in the absence of substantial Tomalchev-Anderson renormalization) and the bandwidth ($W \rightarrow ZW$, where the quasi-particle residue, $Z \ll 1$), due to Brinkman-Rice physics³¹. The Jahn-Teller modes induce an “inverse Hund’s” coupling via the dynamical Jahn-Teller effect that provides the attractive pairing glue for local Cooper pairs. Crucially, as the Jahn-Teller interaction is “traceless” with respect to the charged degrees of freedom, the suppression of charge fluctuations due to Mott physics does not affect the attractive inverse Hund’s coupling, as opposed to electron-phonon interactions with Ag modes which couple to the density³¹: strong electron-phonon interactions and electronic correlations work cooperatively to lead to a $T_c \sim 20K$.

In light of the centrality of Mott physics to superconductivity in K_3C_{60} , we carry out the mapping of our minimal model to K_3C_{60} from an unconventional but incisive vantage point, starting neither from vanilla DFT models of the electronic structure of K_3C_{60} nor from the molecular limit but instead interpreting directly the state-of-the-art DFT+DMFT calculations that account explicitly for Mott effects⁵². The DMFT modified spectral function near the Fermi energy contains two sharp peaks—dramatically sharper than in DFT—which we associate with two partially filled, narrow t_{1u} bands crossing the Fermi surface and one empty, narrow t_{1u} band. As the two peaks in the Mott modified spectral function barely overlap—and do so far from the Fermi energy—we make contact with K_3C_{60} by identifying the lower c band in our model with the two half-filled t_{1u} bands crossing the Fermi surface and the upper d band with the empty t_{1u} band as shown in Fig. 1(b). We map ΔE in our model to the separation of the centers between the two sharp spectral peaks. To summarize, as a first approximation, we assume that the Mott physics in K_3C_{60} acts simply to renormalize the repulsive interaction and electronic spectral features such as the bandwidth and band-splitting—beyond this, the superconductivity is determined by local electron-phonon physics.

Having made these identifications on the electronic side, we note that the Jahn-Teller Hg phonons couple to the t_{1u} bands with different polarizations providing both inter-band and intra-band transitions³¹. Within our effective two-band model, we take polarizations coupling to intra-band transitions to give rise to the equilibrium pairing attraction U_0 that balances the inverse Hund’s coupling with the Mott renormalized Coulomb interaction to give $T_c \sim 20K$, s-wave superconductivity in equilibrium. Inter-band polarizations coupling the half filled bands to the empty bands, give an additional contribution to attraction, $U(Q)$, as we have shown in our model. We note in passing that virtual inter-orbital Cooper tunneling is already believed to play a small contributing role in equilibrium superconductivity^{52,53}, underscoring the interpretation of our microscopics as photo-enhancing a (virtual) Suhl-Kondo effect. Thus, having mapped the intricate, interlacing effects relevant to superconductivity in K_3C_{60} to our minimal, microscopic model, we are now ready to examine the pictures for longevity we provide, starting with photo-induced metastability.

To determine whether a metastable superconducting state exists in K_3C_{60} we take the electron-phonon coupling g for each Hg mode to be consistent with the latest ab-initio calculations⁵⁴ and allow ΔE and $\nu(0)$ to vary due to Mott renormalization. The band gap is rescaled as $\Delta E \rightarrow Z\Delta E$ and $\nu(0) \rightarrow \nu(0)/Z$. We introduce further a U_0 , modulating it as $\nu(0)_{eff}$ changes to keep $\lambda_{eff} = U_0\nu(0)/Z$ constant and thereby $T_c = 20K$ fixed. The optimal mode for photo-induced metastability in K_3C_{60} —possessing both strong electron-phonon coupling and high-frequency—is the Hg(3) mode at 22 THz: the relevant polarization for this mode has $\frac{g\ell_0}{\omega} \approx 0.6$, where ℓ_0 is the effective oscillator length of the phonon. The bare ab-initio DFT density of states is $\nu(0)\omega = 0.603$ and $\Delta E \approx 250$ meV: These are too small to permit photo-induced metastability. However, Nomura et al.⁵² have demonstrated with DMFT + DFT that these values may significantly renormalised with $Z = \frac{1}{2}$. There are reasons to suspect however an even stronger renormalisation with $Z = \frac{1}{5}$: evidence from optical conductivity in the metallic phase show a peak near 50 meV, suggesting a natural experimental measurement of ΔE . 50 meV is a factor of 5 difference from the DFT prediction of the band splitting. For this range of $Z^{-1} = 1 - 5$, we find that Nomura’s data with $Z^{-1} = 2$ puts K_3C_{60} outside the metastable region, while $Z^{-1} \sim 3.34$ would place K_3C_{60} within a metastable regime-I.

Appendix E: Induced attraction from oscillating or fluctuating phonon

In this section we consider a general model including tunneling a q -dependent interactions. This generalisations show that the attraction found in our model is not restricted to the local limit. Moreover, we find that g^4 Schrieffer-Wolff becomes degenerate in the local limit and cannot be carried out perturbatively. As a result, we take the approach

of starting from a full q -dependent model and taking the local q independent limit at the end. We start from the Hamiltonian:

$$H = \sum_k \Delta E_k S_{k,0}^z + 2 \sum_{k,q} g(k,q) Q(q) S_{k,q}^x + \sum_q \frac{M\omega_{ph}^2(q)}{2} Q(q)Q(-q) + \frac{1}{2M} P(q)P(-q). \quad (\text{E1})$$

where ΔE_k is the k -dependent gap between the two bands, $g(q,k)$, the electron-phonon interaction and $\omega(q)$ the phonon dispersion relation.

To remove linear in g terms we use the Schrieffer-Wolff transformation given by:

$$U = e^{iA} = e^{i \sum_{k,q} (\alpha(k,q) S_{k,q}^x P(q) + \beta(k,q) S_{k,q}^y Q(q))}. \quad (\text{E2})$$

This transformation has been previously used in the context of parametric amplification of THz reflectivity in Ta_2NiSe_5 ⁵⁵. The momentum dependent spin density commutators with finite momentum are given by:

$$[S_{k,0}^z, S_{k',q'}^x] = i \frac{\delta_{k,k'} + \delta_{k,k'+q'}}{2} S_{k',q'}^y, \quad (\text{E3})$$

$$[S_{k,0}^z, S_{k',q'}^y] = -i \frac{\delta_{k,k'} + \delta_{k,k'+q'}}{2} S_{k',q'}^x. \quad (\text{E4})$$

With these commutators in place, we find the linear expansion of the Schrieffer-Wolff transformation to be:

$$\begin{aligned} V - i[H_0, A] &= \sum_{k,q} \left(2g(k,q) S_{k,q}^x Q(q) + \frac{\Delta E_k + \Delta E_{k+q}}{2} (\alpha(k,q) S_{k,q}^y P(q) - \beta(k,q) S_{k,q}^x Q(q)) \right. \\ &\quad \left. + M\omega_{ph}^2(q) \alpha(k,q) S_{k,q}^x Q(q) - \frac{1}{M} \beta(k,q) S_{k,q}^y P(q) \right) = 0, \end{aligned} \quad (\text{E5})$$

which leads to the momentum dependent coefficients $\alpha(k,q)$ and $\beta(k,q)$:

$$\alpha(k,q) = \frac{2g(k,q)}{M(\Delta_{k,q}^2 - \omega_{ph}^2(q))}, \quad \beta(k,q) = \frac{2g(k,q)\Delta_{k,q}}{(\Delta E_{k,q}^2 - \omega_{ph}^2(q))}, \quad \text{with} \quad \Delta E_{k,q} = \frac{\Delta E_k + \Delta E_{k+q}}{2}. \quad (\text{E6})$$

The second order Schrieffer-Wolff Hamiltonian is given by:

$$H^{(2)} = -\frac{i}{2} [V, A] = -\frac{i}{2} \sum_{k,q} 2g(k,q) \left[S_{k,q}^x Q(q), \sum_{k',q'} (\alpha(k',q') S_{k',q'}^x P(q') + \beta(k',q') S_{k',q'}^y Q(q')) \right], \quad (\text{E7})$$

$$\begin{aligned} H^{(2)} &= \sum_{k,k',q} (g(k,q) \alpha(k',-q) S_{k,q}^x S_{k',-q}^x) + \sum_{k,k',q,q'} \left(g(k,q) \alpha(k',q') Q(q) P(q') [S_{k,q}^x, S_{k',q'}^x] \right. \\ &\quad \left. + g(k,q) \beta(k',q') Q(q) Q(q') [S_{k,q}^x, S_{k',q'}^y] \right). \end{aligned} \quad (\text{E8})$$

While the above expression looks complicated, we simplify the expression by keeping only independent of d -band operators that correspond to electrons in the unoccupied upper band. We take the local limit for the second order effective interaction, $\lambda(k,q,k',q') = \frac{2g(k,q)g(k',q')\Delta E_{k,q}}{(\Delta E_{k',q'})^2 - \omega_{ph}^2(q')} \approx \frac{2g^2 \Delta E}{(\Delta E)^2 - \omega_{ph}^2}$. Finally, we end up with an effective electron-phonon model only for the lower band:

$$H = \sum_k \xi_k c_k^\dagger c_k + \lambda \sum_{q,q',k} Q(q)Q(q') c_{k+q+q'}^\dagger c_k + \sum_q \frac{M\omega_{ph}^2(q)}{2} Q(q)Q(-q) + \frac{1}{2M} P(q)P(-q). \quad (\text{E9})$$

The above effective Hamiltonian corresponds to an electron-phonon system with an interaction of the type $\lambda Q^2 c^\dagger c$. This observation allows us to make contact with previous work which stipulated such an interaction from phenomenological, symmetry conditions¹³. Here we derive such an interaction from a microscopic electron-phonon model. Moreover perturbation theory indicates that the effective electron-phonon coupling, λ , is resonantly enhanced when

$$\omega_{ph} = \Delta E.$$

The Schrieffer-Wolff necessary to remove the $Q^2 n$ term to linear order and obtain an effective attraction for the electrons is given by:

$$U = e^{iS} = \text{Exp} \left\{ i \sum_{q, q', k} (A(q, q', k) Q(q) P(q') n_{k, q+q'} + B(q, q', k) P(q) P(q') n_{k, q+q'} + C(q, q', k) Q(q) Q(q') n_{k, q+q'}) \right\}, \quad (\text{E10})$$

where we use the notation $n_{q-q'} = \sum_k c_{k+q-q'}^\dagger c_k$ and the commutator of the density operator, $n_{q-q'}$ with the number operator $c_k^\dagger c_k$ is given by:

$$\sum_k \xi_k [c_k^\dagger c_k, n_{k', q+q'}] = (\xi_{k'+q+q'} - \xi_k) n_{k', q+q'} = \omega_{k', q+q'} n_{k', q+q'} \quad (\text{E11})$$

We compute below the transformation to linear order, to fix the parameters $\{A, B, C\}$:

$$\begin{aligned} -i [H_0, S] = & \sum_{q, q', k} \left(-i\omega_{k, q+q'} \left(A(q, q', k) Q(q) P(q') n_{k, q+q'} + \right. \right. \\ & B(q, q', k) P(q) P(q') n_{k, q+q'} + C(q, q', k) Q(q) Q(q') n_{k, q+q'} \left. \right) + \\ & M \frac{(\omega_{ph}^2(-q') + \omega_{ph}^2(q'))}{2} A(q, q', k) Q(q) Q(q') n_{k, q+q'} + \\ & M \frac{(\omega_{ph}^2(-q') + \omega_{ph}^2(q'))}{2} B(q, q', k) Q(q') P(q) n_{k, q+q'} + \\ & M \frac{(\omega_{ph}^2(-q) + \omega_{ph}^2(q))}{2} B(q, q', k) Q(q) P(q') n_{k, q+q'} \\ & - \frac{1}{M} A(q, q', k) P(q) P(q') n_{k, q+q'} \\ & - \frac{1}{M} C(q, q', k) P(q') Q(q) n_{k, q+q'} + \\ & \left. - \frac{1}{M} C(q, q', k) P(q) Q(q') n_{k, q+q'} \right). \end{aligned} \quad (\text{E12})$$

Assuming $\omega(-q) = \omega(q)$. Collecting coefficients of $Q(q)Q(q')n_{k, q+q'}$, $Q(q)P(q')n_{k, q+q'}$, $Q(q)Q(q')n_{k, q+q'}$ and setting them to zero gives rise to the equations:

$$-i\omega_{k, q+q'} (C(q, q', k) + C(q', q, k)) + M\omega_{ph}^2(q) A(q, q', k) + M\omega_{ph}^2(q') A(q', q, k) + \lambda = 0, \quad (\text{E13})$$

$$-i\omega_{k, q+q'} (B(q, q', k) + B(q', q, k)) - \frac{1}{M} (A(q, q', k) + A(q', q, k)) = 0, \quad (\text{E14})$$

$$-i\omega_{k, q+q'} A(q, q', k) + M\omega^2(q) (B(q, q', k) + B(q', q, k)) - \frac{1}{M} (C(q, q', k) + C(q', q, k)) = 0, \quad (\text{E15})$$

$$-i\omega_{k, q+q'} A(q', q, k) + M\omega^2(q') (B(q, q', k) + B(q', q, k)) - \frac{1}{M} (C(q, q', k) + C(q', q, k)) = 0, \quad (\text{E16})$$

which is a system of **four** equations with **four** unknowns $\{A(q, q', k), A(q', q, k), (B(q, q', k) + B(q', q, k)), (C(q, q', k) +$

$C(q', q, k)$ }. Using equation (E15) and (E16), can eliminate $(B(q, q', k) + B(q', q, k))$ and $(C(q, q', k) + C(q', q, k))$:

$$(B(q, q', k) + B(q', q, k)) = \frac{i\omega_{k,q+q'}}{M(\omega_{ph}^2(q) - \omega_{ph}^2(q'))} (A(q, q', k) - A(q', q, k)), \quad (\text{E17})$$

$$2 \frac{(C(q, q', k) + C(q', q, k))}{M} = -i\omega_{k,q+q'} (A(q, q', k) + A(q', q, k)) + \frac{i\omega_{k,q+q'} (\omega_{ph}^2(q) + \omega_{ph}^2(q'))}{\omega_{ph}^2(q) - \omega_{ph}^2(q')} (A(q, q', k) - A(q', q, k)) \quad (\text{E18})$$

Now using equation (E14) we can relate $(A(q, q', k) - A(q', q, k))$ to $(A(q, q', k) + A(q', q, k))$:

$$\frac{\omega_{k,q+q'}^2}{\omega_{ph}^2(q) - \omega_{ph}^2(q')} (A(q, q', k) - A(q', q, k)) = (A(q, q', k) + A(q', q, k)), \quad (\text{E19})$$

Note here that if $\omega_{k,q,q'} = 0$, the symmetric sum is zero, otherwise if $\omega_{ph}(q) = \omega_{ph}(q')$ then the anti-symmetric sum is zero. In terms of the symmetric sum, $(A(q, q', k) + A(q', q, k))$ we can re-write $M\omega_{ph}^2(q)A(q, q', k) + M\omega_{ph}^2(q')A(q', q, k)$ as:

$$M\omega_{ph}^2(q)A(q, q', k) + M\omega_{ph}^2(q')A(q', q, k) = M \left(\frac{\omega_{ph}^2(q) + \omega_{ph}^2(q')}{2} (A(q, q', k) + A(q', q, k)) + \frac{\omega_{ph}^2(q) - \omega_{ph}^2(q')}{2} (A(q, q', k) - A(q', q, k)) \right), \quad (\text{E20})$$

$$= M \left(\frac{\omega_{k,q+q'}^2 (\omega_{ph}^2(q) + \omega_{ph}^2(q')) + (\omega_{ph}^2(q) - \omega_{ph}^2(q'))^2}{2\omega_{k,q+q'}^2} (A(q, q', k) + A(q', q, k)) \right). \quad (\text{E21})$$

Finally, in terms of the symmetric sum $\frac{(C(q,q',k)+C(q',q,k))}{M}$ is given by:

$$\frac{(C(q, q', k) + C(q', q, k))}{M} = \frac{1}{2} \left(-i\omega_{k,q+q'} + \frac{\omega_{ph}^2(q) + \omega_{ph}^2(q')}{-i\omega_{k,q+q'}} \right) (A(q, q', k) + A(q', q, k)), \quad (\text{E22})$$

$$= \frac{-\omega_{k,q+q'}^2 + \omega_{ph}^2(q) + \omega_{ph}^2(q')}{-i2\omega_{k,q+q'}} (A(q, q', k) + A(q', q, k)). \quad (\text{E23})$$

Putting everything together in equation (E13), we find:

$$\frac{1}{2} \left(-\omega_{k,q+q'}^2 + \omega_{ph}^2(q) + \omega_{ph}^2(q') + \frac{\omega_{k,q+q'}^2 (\omega_{ph}^2(q) + \omega_{ph}^2(q')) + (\omega_{ph}^2(q) - \omega_{ph}^2(q'))^2}{\omega_{k,q+q'}^2} \right) (A(q, q', k) + A(q', q, k)) = -\frac{\lambda}{M}, \quad (\text{E24})$$

$$\left(-\omega_{k,q+q'}^2 + 2\omega_{ph}^2(q) + 2\omega_{ph}^2(q') + \frac{(\omega_{ph}^2(q) - \omega_{ph}^2(q'))^2}{\omega_{k,q+q'}^2} \right) (A(q, q', k) + A(q', q, k)) = -\frac{2\lambda}{M} \quad (\text{E25})$$

Here, we see that the dispersion crucially prevents divergences that would prevent us from carrying out the pertur-

bative elimination of the electron-phonon interaction. Now we take the limit of dispersionless phonons and find:

$$A(q, q', k) + A(q', q, k) = -\frac{2\lambda}{M\left(4\omega_{ph}^2 - \omega_{k, q+q'}^2\right)}, \quad (\text{E26})$$

$$B(q, q', k) + B(q', q, k) = -\frac{2i\lambda}{M\left(4\omega_{ph}^2 - \omega_{k, q+q'}^2\right)\omega_{k, q}}, \quad (\text{E27})$$

$$C(q, q', k) + C(q', q, k) = \frac{i\lambda}{M\omega_{k, q}} \quad (\text{E28})$$

$$A(q, q', k) - A(q', q, k) = 0. \quad (\text{E29})$$

In the ultra local limit we find that coefficients B and C diverge invalidating the Schrieffer-Wolff. We construct the final effective Hamiltonian using the A terms in the Schrieffer-Wolff, which give rise to diagonal terms of the type $Q^2 n^2$. We comment here that B and C terms give rise to off-diagonal terms proportional to QP , which we assume to be zero in Gaussian states framework, $\langle QP \rangle = 0$. They also give rise to terms linear in the momentum which corresponds to polarionic renormalisation of the mass of the electrons, but not attraction.

Therefore we focus on the second order in λ Schrieffer-Wolff Hamiltonian given by:

$$-\frac{i}{2}[V, S] = \frac{\lambda}{2} \sum_{q, q', k} \left(Q(q) \sum_{q'', k'} A(q'', -q', k) Q(q'') n_{k', q''-q'} n_{k, q+q'} + Q(q') \sum_{q'', k'} A(q'', -q, k) Q(q'') n_{k', q''-q} n_{k, q+q'} \right). \quad (\text{E30})$$

We decouple the above Hamiltonian within the framework of Gaussian states with homogeneous expectations values. Since within Gaussian states fermion and boson wave functions do not mix, momentum needs to be conserved for boson and fermion independently within each term:

$$Q_q Q_{q'} = Q_q Q_{-q} \delta_{q', -q}. \quad (\text{E31})$$

This leads to the effective phonon mediated attraction Hamiltonian:

$$H_{eff} = \frac{\lambda}{2} \sum_{q, q', k, k'} (Q(q) Q(-q) A(-q, -q', k) n_{k', -q-q'} n_{k, q+q'} + Q(q') Q(-q') A(-q', -q, k) n_{k', -q-q'} n_{k, q+q'}), \quad (\text{E32})$$

$$= \frac{\lambda}{2} \sum_{q, q', k, k'} (Q(q) Q(-q) A(q, q', k) + Q(q') Q(-q') A(q', q, k)) n_{k, q+q'} n_{k', -q-q'}, \quad (\text{E33})$$

$$= \sum_{q, q', k, k'} \frac{\lambda^2 Q_q Q_{-q}}{M(4\omega_{ph}^2 - \omega_{k, q+q'}^2)} n_{k, q+q'} n_{k, -q-q'} \quad (\text{E34})$$

Taking the local limit we find that:

$$H_{eff} = -\frac{2g^4 \Delta E^2}{M\omega_{ph}^2 (\Delta E^2 - \omega_{ph}^2)^2} \sum_{q'} Q_{q'} Q_{-q'} \sum_q n_{\uparrow, q} n_{\downarrow, -q} \quad (\text{E35})$$